Materials Chemistry C

PAPER

View Article Online
View Journal | View Issue

Cite this: *J. Mater. Chem. C*, 2015, 3, 5050

A binary solvent mixture-induced aggregation of a carbazole dendrimer host toward enhancing the performance of solution-processed blue electrophosphorescent devices†

Lihui Liu,‡[a] Xuejing Liu,[ab] Baohua Zhang,*[a] Junqiao Ding,[a] Zhiyuan Xie*[a] and Lixiang Wang[a]

Received 6th March 2015,
Accepted 11th April 2015

DOI: 10.1039/c5tc00625b

www.rsc.org/MaterialsC

The emissive layer morphology strongly correlates with the charge transport and light-emitting performance of solution-processed phosphor-doped organic light-emitting diodes (PhOLEDs). Herein, morphology manipulation of the solution-processed emissive layer comprising of carbazole dendrimer (H2) host:blue phosphor (FIrpic) guest is realized *via* processing of the solvent and its influence on charge transport and light-emitting properties is investigated. The formation of H2 aggregates within its amorphous matrix processed with the toluene:*p*-xylene solvent mixture distinctively improves the hole and electron transport within the emissive layer, helping to lower the driving voltages and improve the light-emitting efficiency. However, excess aggregation of H2 would result in non-uniform dispersion of the FIrpic guest within the H2 host, leading to non-complete host-to-guest energy transfer and decreased electroluminescence performance. Through manipulation of the aggregates within the H2 host by varying the solvent mixture ratio, the trade off between charge transport and energy transfer is realized. Finally, the solution-processed blue PhOLED with optimized emissive layer morphology processed with toluene : *p*-xylene (9 : 1) solvent mixture achieves a high light-emitting efficiency of 27.8 cd A^{-1}, corresponding to 25% enhancement compared to 22.2 cd A^{-1} of the control device processed with commonly used toluene solvent.

Introduction

Solution-processed organic light-emitting diodes have received a great deal of attention because of their compatibility with low-cost and large-area device fabrication approaches such as ink-jet printing or roll-to-roll coating, thus holding great potential for practical application in next generation displays and lightings.[1–3] Among the various approaches developed to date, the host–guest-doping system is the most common strategy to enhance the light-emitting efficiency, in which a conjugated polymer,[4] solution-processable small molecule[5–8] or dendrimer[9] serves as the host and fluorescent or phosphorescent dopant is served as the emitter to form the emissive layer to realize high efficient blue, red, blue and white emissions.[10–13] Some studies have disclosed that the film morphology of the solution-processed multi-component emissive layer strongly influences the final electroluminescence performance of the resultant OLEDs.[14–23] Nevertheless, a report on how to rationally control the morphological feature of those devices is still rare, and the relationship between the film morphology of the multi-component emissive layer and its charge transport properties as well as the resultant device performance is also unclear.[14,18–20]

In contrast to the thermally evaporated counterpart, the morphology of the solution-processed host–guest-doping emissive layer is more complicated. Both the thermodynamic and kinetic factors including miscibility, processing solvent, solution-processing conditions and post-treatment can influence the morphology and the final electroluminescence performance.[8,16–18] An ideal morphology for the host–guest-doping emissive layer requires a uniform dispersion of the dopant within the host matrix to realize efficient energy transfer from host to guest and to suppress exciton quenching. Meanwhile, it requires the emissive layer having high bipolar transporting properties to reduce driving voltage and increase the exciton-forming probability. Some examples have shown that

[a] *State Key Laboratory of Polymer Physics and Chemistry, Changchun Institute of Applied Chemistry, Chinese Academy of Sciences, Changchun 130022, P. R. China. E-mail: bhzhang512@ciac.ac.cn, xiezy_n@ciac.ac.cn*
[b] *University of Chinese Academy of Science, Beijing 100039, P. R. China*

† Electronic supplementary information (ESI) available: AFM and TEM morphology images for the H2: FIrpic (10%, wt%) light-emitting layers. See DOI: 10.1039/c5tc00625b

‡ Present address: Department of Microtechnology and Nanoscience, Quantum Device Physics Laboratory, Chalmers University of Technology, SE-41296 Gothenburg, Sweden.

the aggregation of host materials in virtue of π–π interaction, van der Waals interaction or hydrogen bond interaction has potential to enhance charge transport and lower the driving voltages.[24–27] However, for some solution-processed phosphorescent OLEDs based on small molecule hosts, such as 4,4′,4″-tris(*N*-carbazolyl)-triphenylamine (TCTA),[24] 4,4′-bis(9-carbazolyl)-biphenyl (CBP),[5] 3,6-bis(diphenylphosphoryl)-9-(4′-(diphenylphosphoryl)phenyl)-carbazole (TPCz),[8] it was assumed that the more amorphous morphology of the emissive layer is helpful to improve the light-emitting efficiencies of the resultant OLEDs. This is partly due to the over-aggregation of hosts resulting in incomplete energy transfer or exciton quenching effect. Gong *et al.* have disclosed that the thermo-evaporated TCTA film shows stronger face-to-face π–π stacking and a higher mobility, whereas the spin-coated TCTA film shows amorphous morphology leading to a low charge mobility.[24] Resultantly, their thermo-evaporated OLEDs distinctly outperformed the corresponding solution-processed OLEDs with the same device structure. These results highlight that fine-tuning of the solution-processed emissive layer morphology toward improving charge transport and realizing efficient energy transfer is very crucial for the solution-processed efficient OLEDs.

Very recently, dendrimer host materials have been developed in solution-processed phosphorescent OLEDs.[9,28,29] A dendrimer host is a promising choice for solution-processed OLEDs since it simultaneously possesses the advantages of polymers and small molecules, *i.e.* well-defined chemical structure, high purity, low crystallization trend and excellent film-forming properties. The assembly of dendrimers into supra-molecular structures provides some unique properties and has been applied in sensing, catalysis and nanomedicine fields.[30] However, to the best of our knowledge, there is still no detailed work on the investigation of the morphology issue of dendrimer-based solution-processed OLEDs, in spite of a distinct progress in the device performance of solution-processed OLEDs with this type materials.[6]

Herein, morphology manipulation of the solution-processed emissive layer comprising of carbazole dendrimer (H2)[9,29] host:blue phosphor (FIrpic) guest is realized *via* processing solvents and its influence on charge transport and emissive properties is investigated (see Fig. 1 for chemical structures). The formation of H2 aggregates within its amorphous matrix processed using toluene:*p*-xylene solvent mixture distinctively improves the hole and electron transport within the emissive layer, helping to lower the driving voltages and improve the light-emitting efficiency. However, excess aggregation of H2 would result in non-uniform dispersion of the FIrpic guest within the H2 host, leading to non-complete host-to-guest energy transfer and a decreased electroluminescent performance. Through manipulation of the aggregates within the H2 host by varying the solvent mixture ratio, the tradeoff between charge transport and energy transfer is realized. Finally, the solution-processed blue PhOLED with optimized emissive layer morphology processed with the toluene : *p*-xylene (9 : 1) solvent mixture achieves a high light-emitting efficiency of 27.8 cd A^{-1}, corresponding to 25% enhancement compared to 22.2 cd A^{-1} of the control device processed with the commonly used toluene solvent.

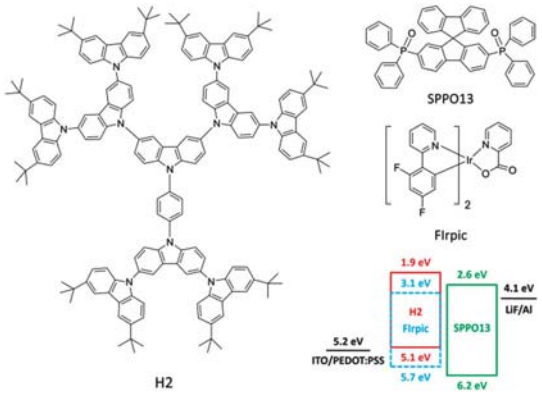

Fig. 1 Chemical structures of the used materials and energy levels diagram of OLEDs.

Experimental

The chemical structures of the used organic materials and the energy level diagram of the solution-processed blue OLEDs are shown in Fig. 1. Poly(ethylenedioxythiophene):poly(styrene sulfonate) (PEDOT:PSS) (Baytron PAI 4083) was purchased from H. C. Starck and used as received. The host material H2, electron transporting material 5,9-di(diphenylphosphineoxide)-9,9′-spirofluorene (SPPO13), and blue phosphorescent iridium(III)-[bis(4,6-difluorophenyl)-pyridinato-*N*,C^2]-picolinate (FIrpic) were synthesized in our lab according to the literature.[29,31,32] The toluene and *p*-xylene solvents were purchased from Aldrich (Purity > 99.8%) and used as received without further purification. The active layer films (pure H2 or H2:FIpric 10 wt%) were prepared *via* spin-coating from their solutions with different solvents and then annealed at 80 °C for 30 min. in nitrogen-filled glove box. Topography images of the films were collected using a SPI3800N atomic force microscopy (AFM) instrument (Seiko Instrument Inc.) in the tapping mode with a 2 N m^{-1} probe and at a scan rate of 1 Hz under ambient conditions. Transmission electron microscopy (TEM) measurements were carried out on a JEOL JEM-1011 TEM operated at an acceleration voltage of 100 kV. The UV-vis absorption spectra were recorded using a Lambda750 spectrometer (Perkin-Elmer, Wellesley, MA) with 5.0 nm slit, and the photoluminescence (PL) spectra were recorded using a Perkin-Elmer LS 50B spectrofluorometer. Grazing incidence X-ray diffraction (GIXRD) was performed using a diffractometer D8 Discover (Bruker, Germany) (λ = 1.54 Å).

The solution-processed blue phosphorescent OLEDs have a structure of indium tin oxide (ITO)/PEDOT:PSS (40 nm)/H2:FIrpic (10 wt%, 45 nm)/SPPO13 (40 nm)/LiF (1 nm)/Al (150 nm). The hole- and electron-only devices have been fabricated with structures of ITO/PEDOT:PSS (40 nm)/H2 (80 nm)/MoO_3 (10 nm)/Al (150 nm) and Al (80 nm)/H2 (80 nm)/Ca (5 nm)/Al (150 nm), respectively. The device fabrication conditions were similar to those reported studies.[16,17] The current–voltage–luminance (*J*–*V*–*L*) characteristics and electroluminescence (EL) spectra were measured using a Keithley 2400 source meter and a coupled PR650 Spectroscan photometer under ambient conditions.

Results and discussion

The pure dendrimer H2 films were prepared *via* spin-coating from various solutions including toluene, *p*-xylene and their mixtures with different volume ratios. Fig. 2 shows the AFM and TEM images of the resultant H2 films from different solvents. As shown in Fig. 2a and e, the H2 film prepared from toluene solution is amorphous. However, for the H2 film prepared with *p*-xylene solution, strong molecule aggregation occurs to form H2 nanofibers within the film as shown in Fig. 2d and h. The width of the nanofibers is about 20 nm derived from the AFM height images in Fig. 2i and k. The distinct morphology difference for H2 films processed with toluene and *p*-xylene is attributed to the different solubilities of H2 in these solvents and the different boiling points of the solvents. The solubility parameters are 18.2 $(\text{mJ m}^{-3})^{1/2}$, 17.9 $(\text{mJ m}^{-3})^{1/2}$ and 18.7 $(\text{mJ m}^{-3})^{1/2}$ for toluene, *p*-xylene and H2, respectively, among which the solubility parameter for H2 was calculated from the cohesive energy density of the functional groups.[33]As compared to toluene, *p*-xylene is a marginal solvent for H2 and H2 molecules tend to aggregate in *p*-xylene.[16] In addition, the boiling point of *p*-xylene is 138 °C, higher than 110 °C of toluene. The low solvent evaporating rate of *p*-xylene also favors to the formation of H2 aggregation compared to the toluene-processed H2 film. The solubility parameter δ_{mix} of a solvent mixture depends on the solubility parameter δ_i and the ratio x_i of each component, $\delta_{\text{mix}} = \Sigma x_i \delta_i$. Thus, through variation of the ratio of toluene and *p*-xylene, the aggregation trend of H2 is assumed to be adjusted. Fig. 2b, c, f and g indicate the AFM and TEM images of the H2 films processed with toluene : *p*-xylene (9 : 1) and toluene : *p*-xylene (5 : 5), respectively. From them we can see that, increasing the content of marginal *p*-xylene increases the aggregation of H2 molecules.

The normalized UV-vis absorption and photoluminescence (PL) spectra of H2 films prepared with different solvents are shown in Fig. 3a. These H2 films show the same deep blue PL emission with the peak located at 406 nm. All kinds of H2 films show similar absorption profiles with distinct absorption peaks located at 287 nm, 298 nm, and 347 nm, respectively. The peak at 298 nm is ascribed to the absorption of the carbazole group ($S_0 \rightarrow S_2$) and the shoulder peak located at 347 nm is assigned to the π–π* transition absorption of the carbazole group ($S_0 \rightarrow S_1$).[25–27] The absorption peaks at 298 nm and 347 nm is sequentially increased upon increasing the *p*-xylene content in the solvent mixtures, suggesting that the π–π interactions between carbazole groups are increased with *p*-xylene processing. The XRD patterns of the H2 films processed with different solvent or solvent mixtures are shown in Fig. 3b. We can see that the H2 film processed with toluene solvent is almost amorphous. When the marginal solvent of *p*-xylene is introduced, the resultant H2 films show a diffraction peak at $2\theta = 6.4^\circ$. The diffraction peak intensity is gradually increased upon increasing the *p*-xylene content in the solvent mixtures, indicating that the H2 molecule aggregation is gradually increased.

The different H2 morphologies may strongly influence its charge-transporting properties. Herein, the hole- and electron-transport characteristics of the H2 films with different morphologies were investigated *via* so-called single carrier devices. Fig. 4a and b show the current density–voltage characteristics of the hole- and electron-only devices with H2 films prepared from different solvents or solvent mixtures, respectively. Except for the H2 films prepared with different solvents or solvent mixtures, all other layers in these devices were fabricated under the same conditions and the detailed fabrication process is described in the Experimental section. Compared to the toluene-processed H2 film,

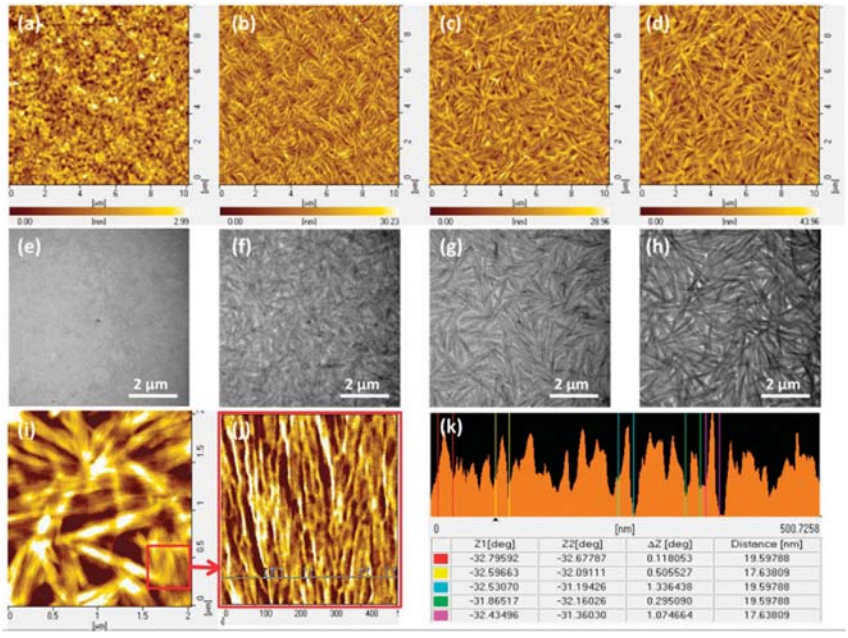

Fig. 2 The AFM (a–d) and TEM (e–h) images for the H2 dendrimers spin-cast from (a, e) toluene, (b, f) toluene : *p*-xylene (9 : 1), (c, g) toluene : *p*-xylene (5 : 5), and (d, h) *p*-xylene solutions. (i, j) The magnified AFM images of the selected area in d. (k) The profiles across the line in j.

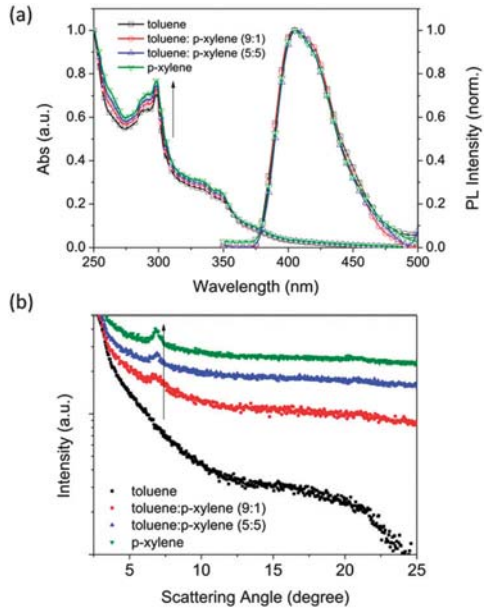

Fig. 3 (a) UV-vis absorption and PL spectra and (b) GIXRD patterns of the H2 films spin-cast from different solvents or solvent mixtures.

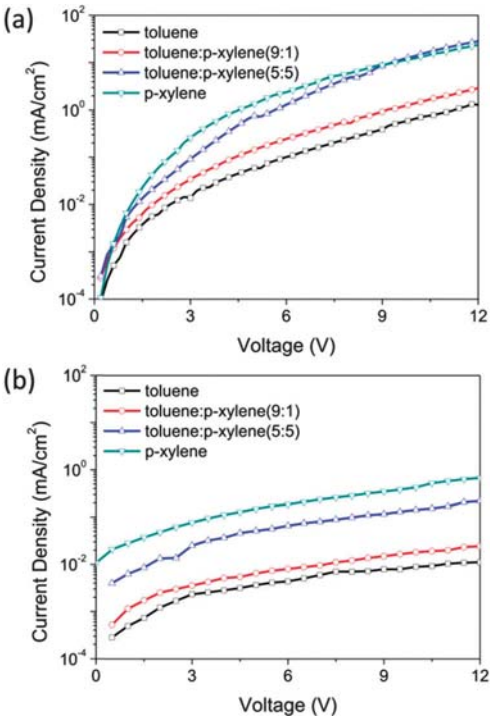

Fig. 4 The current density–voltage characteristics of the (a) hole-only and (b) electron-only devices based on dendrimer H2 films prepared with different solvents or solvent mixtures.

both the electron and hole transport in H2 films are improved when they are prepared with *p*-xylene-containing solvents (see Fig. 4). This is ascribed to the aggregation of H2 molecules in the films with regard to the amorphous H2 morphology processed with toluene. The close packing of H2 molecules in the film and its interconnecting nanofibers facilitate the enhancement of charge transport.[34,35] Along with increasing the H2 aggregation content in the films (see Fig. 2) by increasing the volume content of *p*-xylene, the hole- and electron-transport of the H2 films are gradually increased.

The solution-processed blue phosphorescent OLEDs with the H2:FIrpic (10 wt%) as the emissive layer were fabricated. The emissive layers of H2:FIrpic were spin-coated from the toluene, *p*-xylene and toluene:*p*-xylene solvent mixture, respectively. It is noted here that the doping of FIrpic into the H2 host does not influence the H2 aggregation performance as spin-coated from different solvents or solvent mixtures. The AFM and TEM images of the H2:FIrpic films (shown in the ESI†) show similar morphologies to those of the pure H2 films prepared with different solvents or solvent mixtures shown in Fig. 2. The current density–voltage and current efficiency–luminance characteristics of the solution-processed blue phosphorescent OLEDs based on the emissive layer of H2:FIrpic prepared with these solvents are shown in Fig. 5, and the device parameters are summarized in Table 1. We can see that the light turn-on and driving voltages for the devices with the emissive layer having H2-aggregated morphology (processed with *p*-xylene-containing solvent mixtures) are distinctly lower than those of the control device with an amorphous H2:FIrpic emissive layer (processed with toluene solvent). It is believed that the improved light-emitting performance of the devices is originated from the different solvent-induced emissive layer morphology. As discussed above, the aggregation of H2 host in the emissive layer enhances the charge transport and thus is favorable for lowering the driving

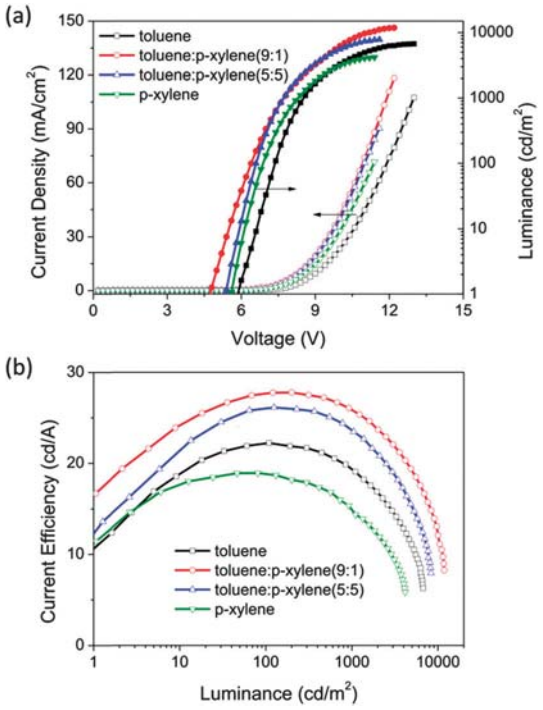

Fig. 5 (a) Current density–luminance–voltage and (b) current efficiency–luminance curves of the solution-processed blue phosphorescent OLEDs with the H2:FIrpic emissive layer processed with toluene, *p*-xylene and toluene:*p*-xylene mixtures, respectively.

Table 1 Summary of the device performance for PhOLEDs fabricated from various solvent

Solvents	V_{on}[a] (V)	Luminance[b] (cd m^{-2})	Current efficiency[b] (cd A^{-1})	Power efficiency[b] (lm W^{-1})	EQE[b] (%)	C.I.E. coordinates (x, y)
Toluene	5.8	6847	22.2	9.5	10.4	0.149, 0.335
Toluene : *p*-xylene (9 : 1)	4.7	11932	27.8	12.7	12.9	0.151, 0.334
Toluene : *p*-xylene (5 : 5)	5.4	8028	26.2	12.3	12.7	0.147, 0.321
p-Xylene	5.6	4250	15.0	9.2	9.4	0.148, 0.314

[a] At a luminance of 1 cd m^{-2}. [b] Peak value.

voltages. As for the current efficiencies of the devices, it is found that the device with the H2:FIrpic emissive layer processed using the toluene : *p*-xylene (9 : 1) solvent mixture obtains the highest efficiency of 27.8 cd A^{-1}, with an increase of 25% compared with 22.2 cd A^{-1} of the control device with the emissive layer processed with toluene. It should be noticed that, among all these devices with different content H2 nanofiber morphology, the device processed with toluene : *p*-xylene (9 : 1) mixture corresponds to the H2 modest self-assembly morphology but displays the best overall device efficiencies. However, further increase of H2 aggregation in the emissive layer decreases the light-emitting efficiencies. The light-emitting efficiencies of the devices processed with toluene : *p*-xylene (5 : 5) and pure *p*-xylene are gradually decreased to 26.2 cd A^{-1} and 15.0 cd A^{-1}, respectively.

In principle, two issues determine the light-emitting efficiencies of the OLEDs. The first is efficient and balanced charge transport in the emissive layer, which favors the increase of the exciton-forming probability on the host. The other is the efficient energy transfer from host to guest. The non-uniform dispersion and aggregation of phosphor guest within the host would result in inefficient energy transfer or triplet exciton quenching leading to a decreased light-emitting efficiency. Herein, the decreased light-emitting efficiencies for the devices based on a strong H2-aggregated emissive layer are assumed to originate from the non-uniform dispersion of FIrpic within the emissive layer. To verify this, the corresponding EL spectra of the resultant blue OLEDs are measured as shown in Fig. 6. We can see that the devices with the H2:FIrpic emissive layer processed with toluene and toluene : *p*-xylene (9 : 1) show pure blue emission from FIrpic, indicating efficient energy transfer from H2 host to FIrpic. Upon increasing the H2 aggregation in the emissive layer, the resultant devices processed with toluene : *p*-xylene (5 : 5) and xylene show gradually increased H2 host emission, indicating non-complete energy transfer from H2 host to FIrpic emitter. This verifies that the decreased light-emitting efficiency is due to the H2 host aggregation-induced non-complete energy transfer. It is reasonable that strong H2 aggregation would push the FIrpic dopant non-uniformly dispersed within the H2 matrix. In other words, the charge transport in the dendritic H2 host matrix and the energy transfer from the H2 host to the FIrpic dopant should be a good trade-off by manipulating the emissive layer morphology toward improving the light-emitting efficiency. Once the domain size of H2 and/or FIrpic is larger than the energy transfer radius, the inefficient energy transfer would decrease the light-emitting efficiency.

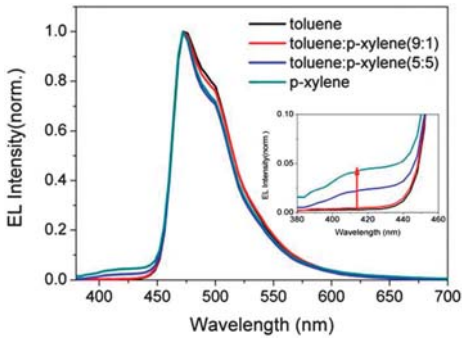

Fig. 6 EL spectra of the solution-processed blue phosphorescent OLEDs with the H2:FIrpic emissive layer processed with toluene, *p*-xylene and toluene:*p*-xylene mixtures, respectively.

Conclusions

In summary, efficient solution-processed blue phosphorescent OLEDs based on the H2:FIrpic emissive layer are fabricated by manipulating the H2 molecule aggregation. The formation of H2 aggregates within its amorphous matrix processed with toluene:*p*-xylene solvent mixture distinctively improves the hole and electron transport within the emissive layer, helping to lower the driving voltages and improve the light-emitting efficiency. However, excess aggregation of H2 would result in a non-uniform dispersion of the FIrpic guest within the H2 host, leading to non-complete host-to-guest energy transfer and a decreased electroluminescent performance. Through manipulation of the aggregates within the H2 host by varying the solvent mixture ratio, the trade off between charge transport and energy transfer is realized. Finally, the solution-processed blue phosphorescent OLED with an optimized emissive layer morphology processed with a toluene:*p*-xylene solvent mixture achieves a high light-emitting efficiency of 27.8 cd A^{-1}. Moreover, the non-chlorinated solvent processing for the emissive layer is in accord with the requirement for the commercialization of solution-processed OLEDs.

Acknowledgements

Z.-Y. X and B.-H. Z acknowledge financial support from the National Basic Research Program of China (2014CB643504) and the National Natural Science Foundation of China (No. 51325303, 51473162 and 21334006). The financial support of the Strategic Priority Research Program of the Chinese Academy of Sciences (XDB12030200) is also acknowledged.

Notes and references

1 S. Xia, K.-O. Cheon, J. J. Brooks, M. Rothman, T. Ngo, P. Hett, C. Raymond, R. C. Kwong, M. Inbasekaran, J. J. Brown, T. Sonoyama, M. Ito, S. Seki and S. Miyashita, *J. Residuals Sci. Technol.*, 2009, **17**, 167–172.
2 S. Reineke, M. Thomschke, B. Lüessem and K. Leo, *Rev. Mod. Phys.*, 2013, **85**, 1245–1293.
3 K. T. Kamtekar, A. P. Monkman and M. R. Bryce, *Adv. Mater.*, 2010, **22**, 572–582.
4 H. B. Wu, J. H. Zou, F. Liu, L. Wang, A. Mikhailovsky, G. C. Bazan, W. Yang and Y. Cao, *Adv. Mater.*, 2008, **20**, 696–702.
5 M. Cai, T. Xiao, E. Hellerich, Y. Chen, R. Shinar and J. Shinar, *Adv. Mater.*, 2011, **23**, 3590–3596.
6 B. H. Zhang, L. H. Liu and Z. Y. Xie, *Isr. J. Chem.*, 2014, **54**, 897–917.
7 Q. Fu, J. S. Chen, C. S. Shi and D. G. Ma, *ACS Appl. Mater. Interfaces*, 2012, **4**, 6579–6586.
8 L. H. Liu, X. J. Liu, K. Q. Wu, J. Q. Ding, B. H. Zhang, Z. Y. Xie and L. X. Wang, *Org. Electron.*, 2014, **15**, 1401–1406.
9 B. H. Zhang, G. P. Tan, C. S. Lam, B. Yao, C. L. Ho, L. H. Liu, Z. Y. Xie, W. Y. Wong, J. Q. Ding and L. X. Wang, *Adv. Mater.*, 2012, **24**, 1873–1877.
10 S. L. Gong, Q. Fu, Q. Wang, C. L. Yang, C. Zhong, J. G. Qin and D. G. Ma, *Adv. Mater.*, 2011, **23**, 4956–4959.
11 S. L. Gong, C. L. Yang and J. G. Qin, *Chem. Soc. Rev.*, 2012, **41**, 4797–4807.
12 S. L. Gong, Q. Fu, W. X. Zeng, C. Zhong, C. L. Yang, D. G. Ma and J. G. Qin, *Chem. Mater.*, 2012, **24**, 3120–3127.
13 C. Fan, Y. H. Li, C. L. Yang, H. B. Wu, J. G. Qin and Y. Cao, *Chem. Mater.*, 2012, **24**, 4581–4587.
14 Y. Y. Noh, C. L. Lee, J. J. Kim and K. Yase, *J. Chem. Phys.*, 2003, **118**, 2853–2864.
15 T. H. Kim, H. K. Lee, O. O. Park, B. D. Chin, S. H. Lee and J. K. Kim, *Adv. Funct. Mater.*, 2006, **16**, 611–617.
16 L. H. Liu, K. Q. Wu, J. Q. Ding, B. H. Zhang and Z. Y. Xie, *Polymer*, 2013, **54**, 6236–6241.
17 L. H. Liu, B. H. Zhang, Z. Y. Xie, J. Q. Ding and L. X. Wang, *Org. Electron.*, 2013, **14**, 55–61.
18 B.-Y. Yu, C.-H. Kuo, W.-B. Wang, G.-J. Yen, S.-I. Iida, S.-Z. Chen, W.-C. Lin, S.-H. Lee, W.-L. Kao, C.-Y. Liu, H.-Y. Chang, Y.-W. You, C.-J. Chang, C.-P. Liu, J.-H. Jou and J.-J. Shyue, *Analyst*, 2011, **136**, 716–723.
19 B.-Y. Yu, C.-Y. Liu, W.-C. Lin, W.-B. Wang, I. M. Lai, S.-Z. Chen, S.-H. Lee, C.-H. Kuo, W.-L. Kao, Y.-W. You, C.-P. Liu, H.-Y. Chang, J.-H. Jou and J.-J. Shyue, *ACS Nano*, 2010, **4**, 2547–2554.
20 K.-H. Yim, W. J. Doherty, W. R. Salaneck, C. E. Murphy, R. H. Friend and J.-S. Kim, *Nano Lett.*, 2010, **10**, 385–392.
21 K.-H. Yim, Z. Zheng, R. H. Friend, W. T. S. Huck and J.-S. Kim, *Adv. Funct. Mater.*, 2008, **18**, 2897–2904.
22 Y. J. Xia and R. H. Friend, *Adv. Mater.*, 2006, **18**, 1371–1376.
23 J. S. Kim, P. K. H. Ho, C. E. Murphy and R. H. Friend, *Macromolecules*, 2004, **37**, 2861–2871.
24 X. Xing, L. Zhong, L. Zhang, Z. Chen, B. Qu, E. Chen, L. Xiao and Q. Gong, *J. Phys. Chem. C*, 2013, **117**, 25405–25408.
25 E. Fisslthaler, A. Blumel, K. Landfester, U. Scherf and E. J. W. List, *Soft Matter*, 2008, **4**, 2448–2453.
26 Z. Ding, R. Xing, Y. Sun, L. Zheng, X. Wang, J. Ding, L. Wang and Y. Han, *RSC Adv.*, 2013, **3**, 8037–8046.
27 Z. Ding, R. Xing, X. Wang, J. Ding, L. Wang and Y. Han, *Soft Matter*, 2013, **9**, 10404–10412.
28 S.-H. Hwang, C. N. Moorefield and G. R. Newkome, *Chem. Soc. Rev.*, 2008, **37**, 2543–2557.
29 J. Q. Ding, B. H. Zhang, J. H. Lü, Z. Y. Xie, L. X. Wang, X. B. Jing and F. S. Wang, *Adv. Mater.*, 2009, **21**, 4983–4986.
30 D. Astruc, E. Boisselier and C. Ornelas, *Chem. Rev.*, 2010, **110**, 1857–1959.
31 S. E. Jang, C. W. Joo and J. Y. Lee, *Thin Solid Films*, 2010, **519**, 906–910.
32 S. Lamansky, P. Djurovich, D. Murphy, F. Abdel-Razzaq, H.-E. Lee, C. Adachi, P. E. Burrows, S. R. Forrest and M. E. Thompson, *J. Am. Chem. Soc.*, 2001, **123**, 4304–4312.
33 A. F. M. Barton, *Handbook of Solubility Parameters and Other Cohesion Parameters*, CRC Press, Boca Raton, FL, 1983.
34 J. M. Lupton, I. D. W. Samuel, R. Beavington, M. J. Frampton, P. L. Burn and H. Bässler, *Phys. Rev. B: Condens. Matter Mater. Phys.*, 2001, **63**, 155206.
35 J. M. Lupton, I. D. W. Samuel, R. Beavington, P. L. Burn and H. Bässler, *Adv. Mater.*, 2001, **13**, 258–261.